Mechanics of Materials 41 (2009) 954–968

Contents lists available at ScienceDirect

Mechanics of Materials

journal homepage: www.elsevier.com/locate/mechmat

# A synergistic damage mechanics approach for composite laminates with matrix cracks in multiple orientations

Chandra Veer Singh, Ramesh Talreja *

*Department of Aerospace Engineering, Texas A&M University, 736A H.R. Bright Building, 3141 TAMU, College Station, TX 77843-3141, USA*

ARTICLE INFO

*Article history:*
Received 22 September 2008
Received in revised form 27 February 2009

ABSTRACT

This paper treats the problem of elastic response of composite laminates containing matrix cracks in plies of multiple orientations. The approach taken has been described as synergistic damage mechanics (SDM) and has been previously illustrated for $[0_m/\pm\theta_n/0_{m/2}]_s$ laminates with cracks of equal density in $+\theta$ and $-\theta$ plies [Singh, C.V., Talreja, R., 2008. Int. J. Solids Struct. 45(16), 4574–4589]. The current work extends the approach to $[0_m/\pm\theta_n/90_r]_s$ and $[0_m/90_r/\pm\theta_n]_s$ laminates with cracks additionally in the 90°-plies. The interaction between the $\pm\theta$-cracks and the 90°-cracks is analyzed in terms of the crack surface displacements using a three-dimensional finite element (FE) model and found to be significant only for crack orientations close to 90°. The stiffness degradation of the laminate with all cracking modes simultaneously present is formulated by continuum damage mechanics using a second order tensor characterization of damage. The elastic moduli changes predicted by the SDM procedure are validated by independent three-dimensional FE calculations. For a particular case of quasi-isotropic $[0/90/\mp45]_s$ laminate, the elastic moduli predictions are evaluated against experimental data. Finally, a parametric study is performed to examine the effects of ply thickness changes on stiffness properties.

Published by Elsevier Ltd.

## 1. Introduction

Efficient use of composite laminates in a wide range of applications requires placing plies in multiple orientations. A common example is a class of laminates called quasi-isotropic that usually have ply orientations of 0°, 45° and 90°, exemplified by the $[0/\pm45/90]_s$ configuration. In spite of such laminates already in use, there is no rigorous and comprehensive analysis available to assess their response in the presence of cracking in more than one set of plies. The need for such analysis in the context of durability and life prediction has been emphasized in a recent report by National Research Council (2005). Lacking such analysis, the current design procedures are conservative, often relying on criteria that allow no cracking at all. To remedy this situation we require an approach that is capable of incorporating effects of ply level (microscopic) failure events into a laminate level (mesoscopic) constitutive framework suited for structural analysis under general loading. One approach of this nature is Synergistic Damage Mechanics (SDM) that retains the Continuum Damage Mechanics (CDM) framework at the mesoscopic level of a representative volume element (RVE) while incorporating microscopic cracking through tensor-valued internal damage variables. Previous works have applied this approach to ply cracks in two symmetrically placed orientations in $[0_m/\pm\theta_n/0_{m/2}]_s$ laminates (Varna et al., 1999; Singh and Talreja, 2008); the present work treats the more general case of $[0_m/\pm\theta_n/90_r]_s$ and $[0_m/90_r/\pm\theta_n]_s$ configurations where cracks are additionally present in the 90°-plies.

The literature in damage mechanics of composite materials is extensive. Rather than cite all approaches, we shall outline those developments that are of direct relevance to treating ply cracking in off-axis orientations. The complexity of cracking in general off-axis orientations has been documented in several experimental studies, e.g., Masters and Reifsnider (1982); O'Brien and Hooper (1993); Tong et al. (1997a); Varna et al. (1999). Analytical methods for

* Corresponding author. Tel.: +1 979 458 3256; fax: +1 979 845 6051.
*E-mail addresses:* chandraveer@tamu.edu (C.V. Singh), talreja@aero.tamu.edu (R. Talreja).

0167-6636/$ - see front matter Published by Elsevier Ltd.
doi:10.1016/j.mechmat.2009.02.008

estimating elastic properties of laminates with distributed off-axis cracks are mostly accurate for transverse cracks in cross ply laminates. More general laminates with cracks require a three-dimensional stress analysis, and efforts to address these situations have typically resorted to either computational methods, e.g. the finite element method (Tong et al., 1997b), or to different approximate methods, e.g., the equivalent constraint method (Zhang et al., 1992) and its combination with modified shear lag theory (Kashtalyan and Soutis, 2000b) or the first-order shear deformation laminate plate theory (Zhang and Herrmann, 1999). More recently, a modified two-dimensional shear lag approach has also been attempted (Yokozeki and Aoki, 2005) for analysis of obliquely crossed cracks. The damage patterns in multidirectional laminates have complexities of geometry as well as interactions between damage modes, examples of which can be found in Kashtalyan and Soutis (2000a,c). Consequently, all approaches by necessity introduce simplifications and develop approximate analyses. Assessment of the approximations becomes difficult when the simplifications reduce the dimensionality of the problem such as going from a three-dimensional geometry of cracks to their two-dimensional projection.

Another approach to formulating constitutive relationships for laminates with cracks was proposed by Gudmundson and Ostlund (1992), and Gudmundson and Zang (1993), in which the crack surface displacements enter explicitly. These displacements were, however, evaluated for a transversely isotropic medium of infinite extent. For thin laminates this approximation introduces approximations that cannot be evaluated in all cases. Lundmark and Varna (2005) improved this situation by reformulating the constitutive relationships for the in-plane loading case in the framework of laminate plate theory. This allowed explicit incorporation of cracking in plies, displaying different effects of cracked outer versus inner plies in a laminate. The crack surface displacements were calculated by using a finite element model and these quantities were expressed by power law relationships in the laminate parameters. Comparisons of the thermal expansion coefficient, longitudinal Young's modulus and major Poisson's ratio for laminates with cracks only in 90°-plies showed good agreement with experimental data. In a continued effort, Lundmark and Varna (2006) included crack sliding displacement of 90° cracks and showed that for one set of cracks the calculated shear modulus of laminates compared favorably with directly evaluated finite element values.

The CDM framework, although quite general and well suited for structural analysis, needs, in its conventional form determination of material coefficients for each laminate configuration. The SDM methodology was proposed (Talreja, 1996) to alleviate this problem by determining these coefficients for a reference configuration (typically a cross ply laminate) and deriving the coefficients for other cases via a "constraint" parameter that is given by relative crack surface displacements evaluated numerically by a finite element model of an appropriate representative volume. The micro-level evaluation of the constraint parameter, which carries the effect of the plies neighboring the cracking plies on the crack surface displacements, provides a convenient way of incorporating the essential effect of cracks on changing the laminate response.

The previous work (Singh and Talreja, 2008) on $[0_m/\pm\theta_n/0_{m/2}]_s$ laminates with cracks in $+\theta$ and $-\theta$ plies showed successful prediction of stiffness coefficients by the SDM methodology. The crack density and the constraint to crack surface displacements in the two orientations were the same in that laminate configuration. Thus, taken together the two sets of cracks acted effectively as one mode of damage. In the current work, the $[0_m/\pm\theta_n/90_r]_s$ and $[0_m/90_r/\pm\theta_n]_s$ configurations analyzed contain cracks additionally in the 90°-plies, providing a truly multimode damage scenario and rendering the generalization of the previous work nontrivial. In the following sections, we shall first present the formulation of stiffness–damage relationships for multimode damage and specialize it to the case of $\pm\theta$-ply damage and 90°-ply damage as the two damage modes in the selected configurations. The constraint parameters appearing in these relationships will be defined in terms of the crack opening displacements (CODs) in a given damage mode. A 3-D finite element (FE) based procedure for calculating the CODs in a representative unit cell will be described next. The SDM methodology will be described and its predictions of axial modulus and the Poisson's ratio for increasing crack densities will be compared with the moduli computed independently by the FE model. The experimental data for the case of a quasi-isotropic $[0/90/\mp 45]_s$ laminate will be compared with the SDM predictions. Finally, the effect of ply thickness in cracked versus uncracked plies will be illustrated by a limited parametric study.

## 2. Stiffness relations for $[\mathbf{0_m/\pm\theta_n/90_r}]_s$ and $[\mathbf{0_m/90_r/\pm\theta_n}]_s$ laminates

### 2.1. Matrix cracking in multiple off-axis plies

Consider a laminate with a mix of on-axis and off-axis plies loaded axially, i.e. along the direction of fibers in the on-axis plies. Such a laminate is illustrated in Fig. 1. Let the off-axis ply orientations be denoted by $\theta_1, \theta_2$, etc. The in-plane stress state in each of these plies with respect to the material axes is displayed in the figure. This stress state can attain a critical value for matrix cracking in one of the off-axis plies at an applied load, and with further increase of the load, multiple matrix cracking can ensue by the so-called shear-lag process. Similarly, the crack initiation and multiplication process in other off-axis plies can occur at different applied load values. Defining the set of intralaminar multiple cracks of a given orientation ($\theta_1, \theta_2$, etc.) as a damage mode, a load-induced multi-mode damage scenario can develop. To be sure, such a scenario is also possible under thermal loading (e.g. cooldown from curing temperature) or under a combined thermal and mechanical loading.

Since laminates are often designed to have plies aligned with the anticipated major load direction in order to sustain that load, while the off-axis plies are placed to provide the needed shear and transverse stiffness, the choice of $[0_m/\pm\theta_n/90_r]_s$ and $[0_m/90_r/\pm\theta_n]_s$ laminates for damage analysis presented here is intended to address many prac-

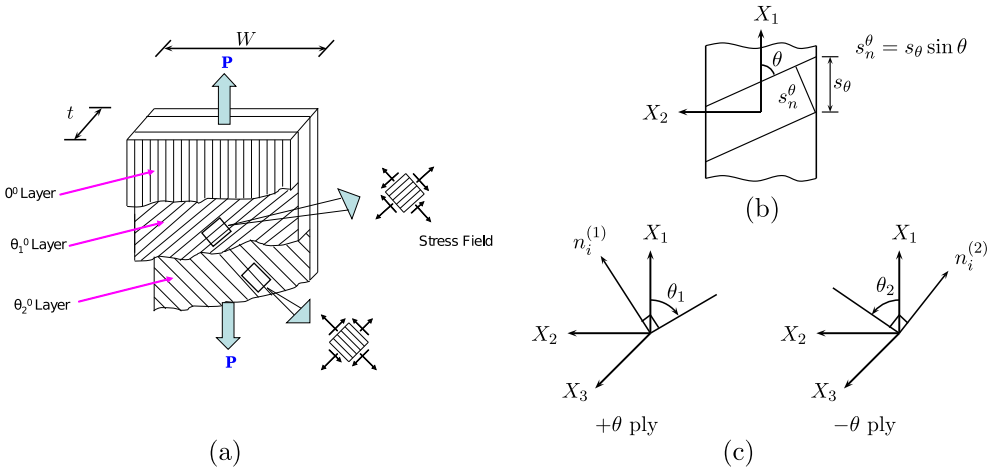


**Fig. 1.** A general half-laminate with off-axis plies: (a) geometry and loading, (b) normal crack spacing $s_n^\theta$, and axial crack spacing $s_\theta$ in a cracked ply, and (c) directions of normal vectors for cracks in $+\theta$ and $-\theta$ plies.

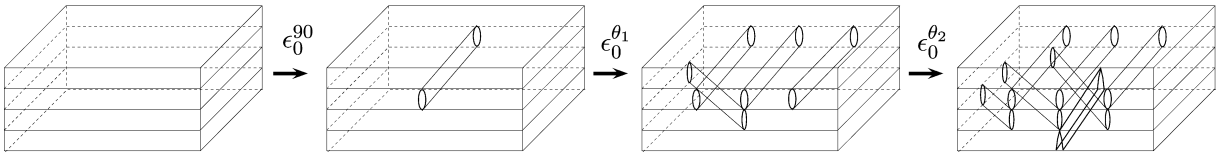


**Fig. 2.** Cracking process in $[0/90/\theta_1/\theta_2]_s$ half-laminate.

tical situations. Fig. 2 illustrates the development of multiple damage modes in these laminate configurations under an axial tensile load. As indicated there, cracking initiates first in the 90°-plies at an overall strain $\epsilon_0^{90}$, and on increasing the load, this cracking multiplies. At the strain $\epsilon_0^{\theta_1}$ the $\theta_1$-plies begin cracking and with further increase in the imposed load, an interactive cracking process continues in both ply orientations. Eventually, all off-axis plies can conduct the multiple cracking process. In the special case where two ply orientations have the same, or nearly the same, conditions (constraints) for cracking, two cracking modes can occur simultaneously. In earlier works (Varna et al., 1999; Singh and Talreja, 2008) it was found that in $[0_m/\pm\theta_n/0_{m/2}]_s$ laminates the crack densities in the $+\theta$ and $-\theta$ orientations could be assumed to be the same and their combined effect could be represented by a single equivalent damage mode. For the $[0_m/\pm\theta_n/90_r]_s$ and $[0_m/90_r/\pm\theta_n]_s$ laminates, we shall show later that the cracking of the $\pm\theta$-plies here also with good approximation can be represented by one damage mode. Thus the total damage description in these laminates would require adding the 90°-ply cracking as a separate damage mode.

### 2.2. Damage characterization and elastic response for two damage modes

Assuming that there are $N$ damage entities of a given damage mode $\alpha$ in the RVE, the normal part of damage tensor is taken as (Talreja, 1990, 1994)

$$D_{ij}^{(\alpha)} = \frac{1}{V}\sum_{k_\alpha}\left[\int_S a n_i n_j \mathrm{d}S\right]_{k_\alpha} \tag{1}$$

where $n_i = (\sin\theta, \cos\theta, 0)$ are components of the unit vector normal to a matrix crack plane in the off-axis ply of orientation $\theta$ with respect to laminate longitudinal axis, $V$ is volume of RVE and $k_\alpha = 1, 2, \ldots, N$. The surface area of a crack, $S$, and the influence vector magnitude, $a$, are specified as

$$S = \frac{t_c \cdot W}{|\sin\theta|} \tag{2}$$

$$a = \kappa . t_c \tag{3}$$

where $\kappa$, called the constraint parameter, is an unspecified constant of (assumed) proportionality between $a$ and the crack size $t_c$ (also cracked-ply thickness), and $W$ is the laminate width (Fig. 1). Assuming $a$ to be constant over the crack surface, one gets from Eq. (1)

$$D_{ij}^{(\alpha)} = \frac{\kappa t_c^2}{s_\theta t \sin\theta} n_i n_j \tag{4}$$

where $s_\theta$ is the axial crack spacing in the cracked ply. The elastic stiffness tensor of the damaged laminate for in-plane response can be expressed as (see the derivation in the Appendix: Eq. (A-7))

$$C_{pq} = C_{pq}^0 + \sum_\alpha C_{pq}^{(\alpha)} \tag{5}$$

where $p, q = 1, 2, 6$, $C_{pq}^0$ is the stiffness coefficient matrix of the virgin laminate and $\sum_\alpha C_{pq}^{(\alpha)}$ represents the total stiffness change due to all modes of matrix cracking averaged over the RVE.

Following the usual CDM procedure (see Appendix for details of derivation of Eqs. (A-37) and (A-38)), the stiffness matrix of the damaged $[0_m/\pm\theta_n/90_r]_s$ laminate can be derived as

$$C_{pq} = \begin{bmatrix} \frac{E_1^0}{1-\nu_{12}^0\nu_{21}^0} & \frac{\nu_{12}^0 E_2^0}{1-\nu_{12}^0\nu_{21}^0} & 0 \\ & \frac{E_2^0}{1-\nu_{12}^0\nu_{21}^0} & 0 \\ Symm & & G_{12}^0 \end{bmatrix} + \overline{D}\begin{bmatrix} 2a_1' & a_4' & 0 \\ & 2a_2' & 0 \\ Symm & & 2a_3' \end{bmatrix} \tag{6}$$

where

$$\overline{D} = \frac{4t_0^2}{t}\left[\frac{1}{s_n^\theta}\frac{\kappa_\theta}{\kappa_\theta|_{\theta=90}}\{(2n+r)^2\kappa_{90_{4n+2r}} - r^2\kappa_{90}\} + r^2\frac{\kappa_{90}}{s^{90}}\right] \tag{7}$$

where $t_0$ is the thickness of a single ply, $s_n^\theta$ and $s^{90}$ are the normal crack spacings in $\pm\theta$ and 90°-plies, respectively, and the constraint parameters are defined as

$$\kappa_\theta = \frac{(\overline{\Delta u_y})_{\pm\theta_{2n}}}{2nt_0}; \quad \kappa_{90_{4n+2r}} = \frac{(\overline{\Delta u_y})_{90_{4n+2r}}}{(4n+2r)t_0}; \quad \kappa_{90} = \frac{(\overline{\Delta u_y})_{90_{2r}}}{2rt_0} \tag{8}$$

where subscript denotes a particular damage mode (orientation of cracked plies) and sub-subscript represents the number of cracked plies corresponding to that damage mode. $\overline{\Delta u_y}$ is the crack opening displacement (COD) averaged over thickness of the cracked ply, and is defined as

$$\overline{\Delta u_y} = \frac{1}{t_c}\int_{-t_c/2}^{t_c/2}\Delta u_y(z)\mathrm{d}z \tag{9}$$

where $\Delta u_y$ represents the separation of crack planes in the direction normal to the crack face with the local coordinate system $(x, y, z)$ placed on the crack as shown in Fig. 3. Since the 90° cracks are centrally placed along the laminate thickness, the crack size for 90° damage mode is $2rt_0$. The average COD in $+\theta$ and $-\theta$ layers are added to yield an equivalent constraint parameter with a crack size of $2nt_0$. The central mode occurs once in the damaged laminate, while the non-central mode occurs twice (on either side of the laminate mid-plane).

The stiffness–damage relationships for $[0_m/90_r/\pm\theta_n]_s$ laminates can be obtained by following the same steps as described above. It must be noted that unlike $[0_m/\pm\theta_n/90_r]_s$ laminates, $\pm\theta$ damage mode in this case is centrally placed, thereby the corresponding equivalent crack size is $4nt_0$ (with averaging over two $+\theta$ and two $-\theta$ layers). On the other hand, the crack size for the 90° damage mode is $rt_0$. The derived stiffness–damage relationships retain the form of Eq. (6). However $\overline{D}$ in this case is given by

$$\overline{D} = \frac{2t_0^2}{t}\left[\frac{1}{s_n^\theta}\frac{\kappa_\theta}{\kappa_\theta|_{\theta=90}}\{2(2n+r)^2\kappa_{90_{4n+2r}} - r^2\kappa_{90}\} + r^2\frac{\kappa_{90}}{s^{90}}\right] \tag{10}$$

with the corresponding constraint parameters given as

$$\kappa_\theta = \frac{(\overline{\Delta u_y})_{\pm\theta_{4n}}}{4nt_0}; \quad \kappa_{90_{4n+2r}} = \frac{(\overline{\Delta u_y})_{90_{4n+2r}}}{(4n+2r)t_0}; \quad \kappa_{90} = \frac{(\overline{\Delta u_y})_{90_r}}{rt_0} \tag{11}$$

From stiffness–damage relationships (Eq. (6)), the engineering moduli for the damaged laminate can now be derived using the following relationships

$$E_1 = \frac{C_{11}C_{22} - C_{12}^2}{C_{22}}; \quad E_2 = \frac{C_{11}C_{22} - C_{12}^2}{C_{11}};$$
$$\nu_{12} = \frac{C_{12}}{C_{22}}; \quad G_{12} = C_{66} \tag{12}$$

Thus,

$$E_1 = \frac{E_1^0}{1-\nu_{12}^0\nu_{21}^0} + 2\overline{D}a_1' - \frac{\left[\frac{\nu_{12}^0 E_2^0}{1-\nu_{12}^0\nu_{21}^0} + \overline{D}a_4'\right]^2}{\frac{E_2^0}{1-\nu_{12}^0\nu_{21}^0} + 2\overline{D}a_2'} \tag{13}$$

$$E_2 = \frac{E_2^0}{1-\nu_{12}^0\nu_{21}^0} + 2\overline{D}a_2' - \frac{\left[\frac{\nu_{12}^0 E_2^0}{1-\nu_{12}^0\nu_{21}^0} + \overline{D}a_4'\right]^2}{\frac{E_1^0}{1-\nu_{12}^0\nu_{21}^0} + 2\overline{D}a_1'} \tag{14}$$

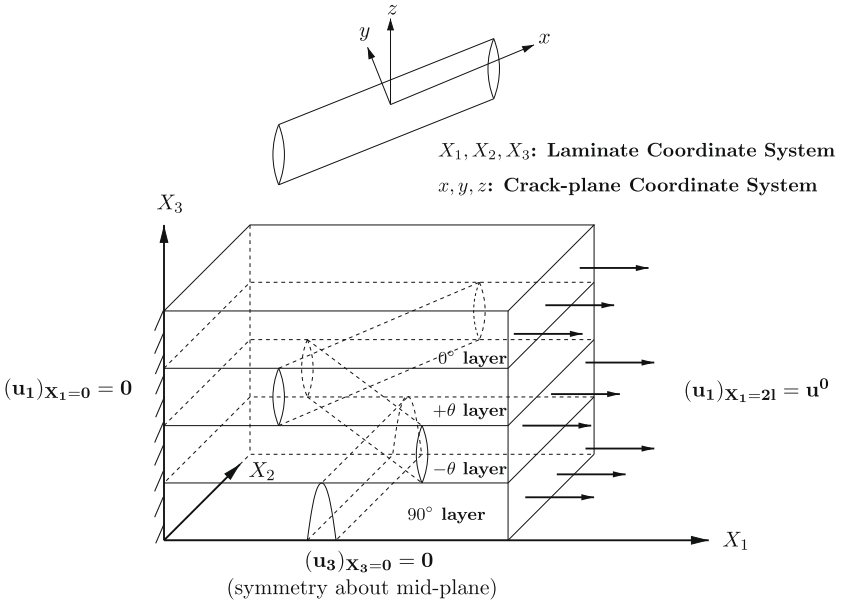


**Fig. 3.** Representative unit cell for FE analysis of $[0_m/\pm\theta_n/90_r]_s$ laminate.

$$\nu_{12} = \frac{\frac{\nu_{12}^0 E_2^0}{1-\nu_{12}^0\nu_{21}^0} + \overline{D}a_4'}{\frac{E_2^0}{1-\nu_{12}^0\nu_{21}^0} + 2\overline{D}a_2'} \tag{15}$$

$$G_{12} = G_{12}^0 + 2\overline{D}a_3' \tag{16}$$

In the above expressions, the constants $a_i', i = 1,2,3,4$ are material constants representing the effect of cracking on laminate stiffness properties. The usual way to obtain them is through experimental data for a selected reference laminate, e.g. a cross ply laminate ($\theta = 90^\circ$), at a certain crack density. However, an alternative and more general way is by numerical simulation, which will be discussed later.

The flow chart in Fig. 4 describes the procedure for multiscale synergistic methodology for multimode damage assessment. Computational micromechanics involves analysis of a representative unit cell to determine the COD values and the constraint parameters. In a separate step, the material constants $a_i'$ appearing in Eqs. (13)–(16) are determined from experiments or numerical simulations carried for a reference laminate, specifically, $[0/90_3]_s$. These relations are then employed to predict stiffness degradation with constraint parameters and material constants obtained from experiments (or FE simulations) as inputs. In the final step, the overall structural behavior in response to external loading can be analyzed based on the degraded stiffness properties for the damaged laminate.

## 3. FE modeling

As described in Section 2, SDM uses micromechanics modeling to evaluate the constraint effects of undamaged plies over cracked plies. Three-dimensional FE analysis is performed here as a micromechanical tool to calculate the constraint parameters. A representative unit cell of the RVE for $[0_m/\pm\theta_n/90_r]_s$ laminate configuration with imposed symmetry boundary conditions is shown in Fig. 3. In FE analyses, the cell size is taken sufficiently large so as to avoid significant interaction between adjacent cracks in an individual ply. Each ply in the laminate is 0.125 mm thick. The ply material is glass-epoxy (HyE 9082Af, Fiberite) with in-plane properties $E_{11} = 44.7$ GPa, $E_{22} = 12.7$ GPa, $G_{12} = 5.8$ GPa and $\nu_{12} = 0.297$. To obtain the remaining properties for use in the 3-D model, the unidirectional ply is assumed transversely isotropic in the cross-sectional plane. Thus, $E_{33} = E_{22} = 12.7$ GPa; $G_{13} = G_{12} = 5.8$ GPa; $\nu_{13} = \nu_{12} = 0.297$; $G_{23} = \frac{E_{22}}{2(1+\nu_{23})} = 4.885$ GPa. The Poisson's ratio $\nu_{23}$ in the isotropic cross-sectional plane is taken as 0.3.

Separate 3-D FE models were constructed for ply orientations, $\theta = 25, 40, 55, 70, 80$ and $90^\circ$, accounting for the mid-plane symmetry. The matrix cracks were taken to have grown across the entire width of the specimen. ANSYS SOLID45 (eight-noded isoparametric) elements were used. Each FE model contained 10,000–50,000 elements to ensure sufficient accuracy of FE computations. A smooth flow of mesh through the thickness was obtained using mapped meshing. Aspect ratio of elements near the crack surfaces was kept close to 1.0 for better accuracy. Linear Elastic FE analyses were carried out on unit cells using ANSYS 10.0 at 0.5 % axial strain. Displacement boundary conditions were applied by constraining the left end of the unit cell and providing required displacement at the right end, such that,

$$(u_1)_{X_1=0} = 0; \quad (u_1)_{X_1=2l} = u^0; \quad (u_3)_{X_3=0} = 0 \ (\textit{symmetry}) \tag{17}$$

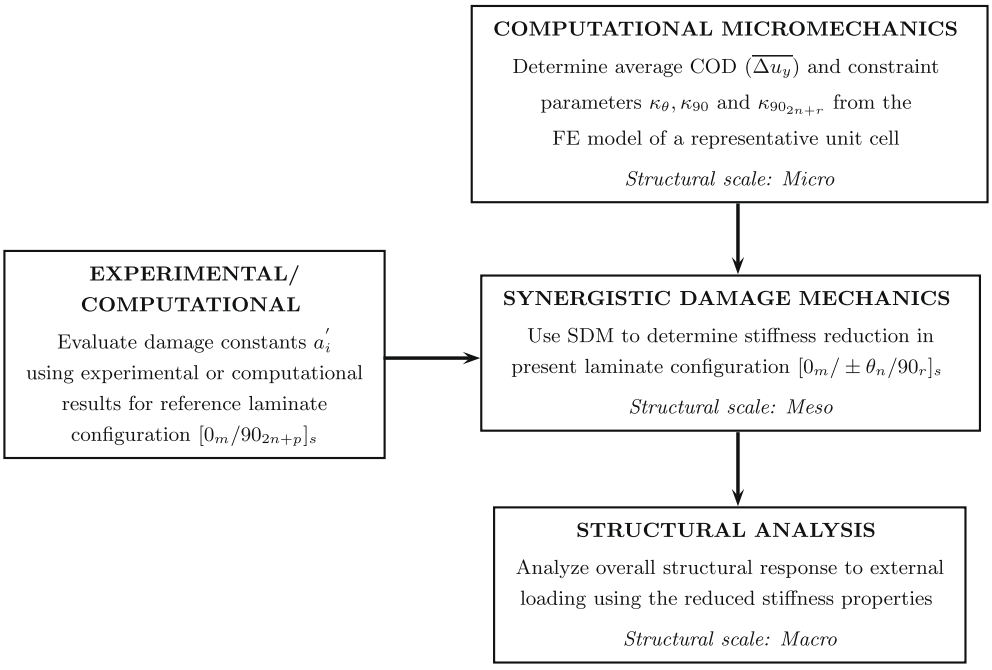


**Fig. 4.** Multi-scale synergistic methodology for analyzing damage behavior in a general symmetric laminate $[0_m/\pm\theta_n/90_r]_s$ with matrix cracks in $+\theta, -\theta$, and $90^\circ$ layers.

where $u^0$ is the applied displacement and $2l$ is the length of unit cell (Fig. 3).

Due to presence of cracked surfaces in three directions ($+\theta, -\theta$ and 90°), it is not possible to construct a fully periodic unit cell for the cracked laminate. Since there is no periodicity in the width direction, the width of the unit cell is chosen large enough such that the errors due to effects from the free edges are negligible. Thus the cell used is not a unit cell, but a "representative" unit cell.

In a real scenario (experiments), the crack spacing may be different in different plies. To account for this, two extreme situations are modeled here. The first case refers to the scenario when cracks in all cracked layers intersect at the same $X_1$ location and hence there is maximum interaction between cracks. The other extreme is when the cracks in different cracked layers are far apart and do not interact. The real behavior will be between the two extremes. The unit cell shown in Fig. 3 actually refers to the first scenario.

## 4. Results and discussion

### 4.1. FE simulations methodology

As can be seen from the flowchart in Fig. 4, SDM requires determination of material constants $a_i'$ from the results for a reference laminate. For the present case of $[0_m/\pm\theta_n/90_r]_s$ laminates, we choose $[0/90_3]_s$, i.e., $\theta = 90^\circ$ and $m = n = r = 1$, as the reference laminate. The stiffness–damage results for this cross-ply laminate can be obtained in a variety of ways. The most obvious way would be by using experimental data. However, although experiments reflect the real material behavior, they can be performed for limited cases. An alternative and more general way is to use a numerical tool such as an FE model to simulate stiffness degradation. FE simulations are in fact easier to carry out and have no scatter other than the accuracy of computations that may depend on mesh density and implementation of boundary conditions. Moreover, they can also be used to predict stiffness changes in other laminate layups. Thus, in what follows next, we will compare SDM predictions with independent FE simulations.

To gain confidence in the above approach for cracked off-axis laminates, we first validated the FE simulations methodology with the experimental data. Using an FE model, stiffness degradation in $[0/\pm\theta_4/0_{1/2}]_s$ glass-epoxy laminates was simulated. The crack density along $X_1$ direction (or equivalently, the crack spacing) was varied by changing the length of the unit cell considered. Linear FE analyses using ANSYS 10.0 were conducted for crack spacing, $s_\theta = 16, 8, 4, 3, 2, 1.5, 1.25, 1, 0.75, 0.6$ and 0.5 mm. The longitudinal modulus and the Poisson's ratio of the damaged laminate were obtained using the volume averaging of stresses and strains as given by the following equations

$$E_1 = \frac{\langle \sigma_{11} \rangle}{\langle \epsilon_{11} \rangle} \tag{18}$$

$$\nu_{12} = -\frac{\langle \epsilon_{22} \rangle}{\langle \epsilon_{11} \rangle} \tag{19}$$

Fig. 5 compares FE simulations with the published experimental data Varna et al. (1999) for $[0/90_8/0_{1/2}]_s$ laminate configuration. As can be seen these simulations show excellent agreement with the experimental data.

### 4.2. SDM predictions

Following the SDM flowchart (Fig. 4), stiffness prediction entails three main steps:

1. Using FE computations, evaluate constraint parameters for each damage mode and the effective damage parameter $\overline{D}$, given by Eqs. (7) and (8).
2. Determinate damage constants $a_i'$ appearing in Eq. (6) using the stiffness degradation data for a pre-selected reference laminate, viz. $[0/90_3]_s$.
3. Predict stiffness changes for $[0_m/\pm\theta_n/90_r]_s$ laminates using the stiffness–damage relations (Eqs. (13)–(16)).

We will describe these steps in the following paragraphs.

#### 4.2.1. CODs and interaction between damage modes

As seen from Eq. (8), the constraint parameters are given as average COD ($\overline{\Delta u_y}$) normalized by crack size (or thickness of the cracked layer). To estimate $\overline{\Delta u_y}$ numerically (Eq. (9)),

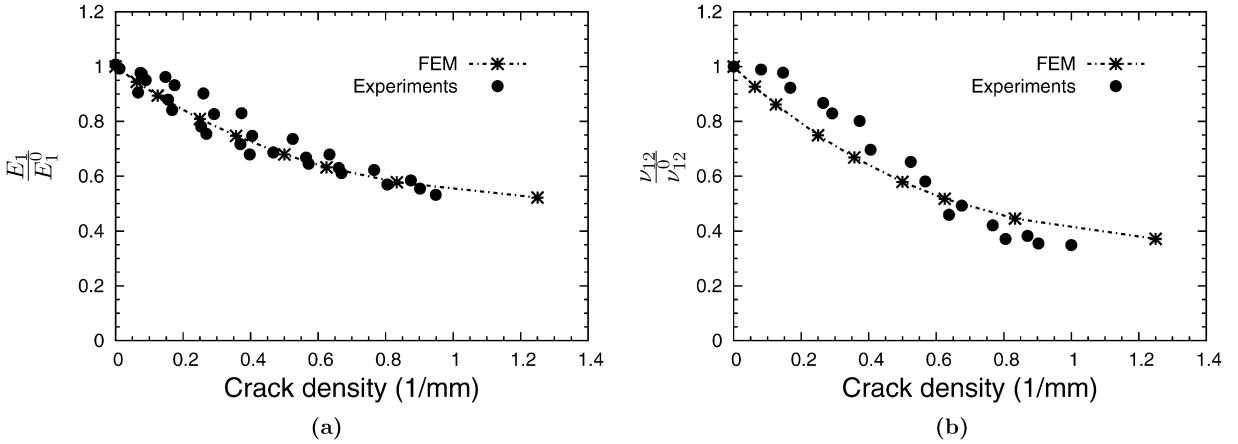


**Fig. 5.** FE simulation of stiffness reduction for $[0/90_8/0_{1/2}]_s$ laminate compared with experimental data Varna et al. (1999).

$\Delta u_y$ is determined from nodal $y$-direction (normal to the crack plane) displacements averaged over the entire crack surface. CODs in two symmetric modes ($+\theta$ and $-\theta$-cracks) are added together to get $\overline{\Delta(u_y)_{\pm\theta}}$ based on an observation in our previous paper (Singh and Talreja, 2008) that these two symmetric damage modes can be added together to yield one equivalent damage mode.

For $[0_m/\pm\theta_n/90_r]_s$ laminates, three cracking modes are present in the damaged material. Due to similarity in the constraining nature and the influence on material response of the cracks in $+\theta$ and $-\theta$ layers, these cracking modes can be coupled together to yield one effective $\pm\theta$-damage mode (see Appendix). However, $\pm\theta$ and 90° cracking modes can interact and influence the stress pattern around cracks in cracked as well as in un-cracked layers, thereby affecting the overall stiffness properties of the cracked laminate. Thus, one needs to incorporate this interaction between different cracking modes into the damage model.

The stiffness–damage relations derived in the present work do not explicitly account for the interaction between different damage modes because the polynomial used for Helmholtz free energy function (Eq. (A-6)) does not contain terms involving product of $D_{ij}^{(\alpha)}$ terms, e.g., $D_1^{(1)}D_1^{(2)}, D_2^{(1)}D_2^{(2)}$, etc. However, the SDM approach provides an indirect means of dealing with intra-mode interaction through calculation of COD using FE model with multi-mode cracks. Let us consider the following two cases

1. No interaction between damage modes: This scenario will exist when the cracks in different damage modes are far apart and thus their mutual interaction is not significant. This can be simulated in the FE model by considering two damage modes separately and then adding (superposing) their effects. Thus, for $[0_m/\pm\theta_n/90_r]_s$ laminate, we carry out COD calculations in two different cracking conditions. In the first case, cracks are present only in $\pm\theta_n$ layers, while in the second case cracks are present only in the $90_r$ layers.
2. Maximum interaction between damage modes: This scenario will occur when the cracks in different damage modes are sufficiently close to cause additional perturbation in the stress fields on top of that due to individual damage modes. The total perturbation effect can be captured in the SDM technique indirectly in the calculated COD when both $\pm\theta_n$ and $90_r$ layers are cracked. The interaction effect is actually observed in experiments, e.g., for $[0/90/-45/45]_s$ laminates, Tong et al. Tong et al. (1997a) observed that $-45°$ cracks grew from the points of intersection of the 90° cracks at the 90°/−45° interface, and +45° cracks initiated at the locations where $-45°$ cracks met the $-45°$/+45° interface. Hence, while modeling multi-mode damage scenario, one should consider these interaction effects.

It is noteworthy here that the two cases represent extremes and the real material behavior is expected to be somewhere in between.

The normalized average CODs for various laminate layups are given in Table 1. The average CODs are nondimensionalized by the cracked-ply thickness ($10^3\frac{\overline{\Delta u_y}}{t_c}$) to give the constraint parameters. The first and the second halves in the table refer to the two cases described above. The columns in the table give the normalized average CODs for layers in this order: $+\theta, -\theta$, their average (i.e., for the combined $\pm\theta$ damage mode), and then 90°. $[0/\pm 90/90]_s$ is just a hypothetical case where cracks are in $\pm 90$ layers. This is done in order to get $\kappa_\theta|_{\theta=90}$ (see Eqs. 7, 8). From the table, it can be observed that the influence of crack interaction is the least for $+\theta$-cracking mode, and the highest for 90° mode. As $\theta$ in $[0_m/\pm\theta_n/90_r]_s$ laminates increases, this interaction becomes increasingly significant. It can also be observed that the interaction is not influential for ply orientations away from 90°. The influence of crack interaction on stiffness changes will be discussed in the following sub-sections.

#### 4.2.2. Calculation of damage constants $a_i'$

In the second step, we obtain damage constants $a_i'$ using the degradation results for the reference laminate configuration $[0/90_3]_s$. Although these results can be taken from experimental data or an analytical model, we use FE for calculation of stiffness changes for this reference laminate configuration as per the discussion above. Using Eq. (6) with $\theta = 90$ and a preselected $s_n^\theta = s^{90} = s_0$, we obtain

$$\begin{bmatrix} \frac{E_1^0}{1-\nu_{12}^0\nu_{21}^0} & \frac{\nu_{12}^0E_2^0}{1-\nu_{12}^0\nu_{21}^0} & 0 \\ & \frac{E_2^0}{1-\nu_{12}^0\nu_{21}^0} & 0 \\ Symm & & G_{12}^0 \end{bmatrix} + \overline{D}_0 \begin{bmatrix} 2a_1' & a_4' & 0 \\ & 2a_2' & 0 \\ Symm & & 2a_3' \end{bmatrix} = \begin{bmatrix} \frac{E_1}{1-\nu_{12}\nu_{21}} & \frac{\nu_{12}E_2}{1-\nu_{12}\nu_{21}} & 0 \\ & \frac{E_2}{1-\nu_{12}\nu_{21}} & 0 \\ Symm & & G_{12} \end{bmatrix} \tag{20}$$

**Table 1**
Normalized average COD $\left(10^3\frac{\overline{\Delta u_y}}{t_c}\right)$.

| Laminate configuration | Non-interacting modes | | | | Interacting modes | | | |
|---|---|---|---|---|---|---|---|---|
| | $+\theta$ layer | $-\theta$ layer | $\pm\theta$ layer | 90° layer | $+\theta$ layer | $-\theta$ layer | $\pm\theta$ layer | 90° layer |
| $[0/\pm 25/90]_s$ | 0.92 | 1.08 | 1.00 | 5.30 | 0.93 | 1.09 | 1.01 | 5.31 |
| $[0/\pm 40/90]_s$ | 2.00 | 2.21 | 2.11 | 5.68 | 2.03 | 2.23 | 2.13 | 5.70 |
| $[0/\pm 55/90]_s$ | 4.38 | 4.66 | 4.52 | 6.31 | 4.83 | 6.05 | 5.44 | 7.50 |
| $[0/\pm 70/90]_s$ | 6.13 | 6.64 | 6.38 | 6.72 | 7.09 | 9.86 | 8.48 | 9.06 |
| $[0/\pm 80/90]_s$ | 7.37 | 8.09 | 7.74 | 6.84 | 8.53 | 12.02 | 10.27 | 9.22 |
| $[0/\pm 90/90]_s$ | – | – | – | – | – | – | 11.44 | – |
| $[0/90_3]_s$ | – | – | – | – | – | – | – | 7.11 |
| $[0_2/\pm 55/90]_s$ | 4.30 | 4.60 | 4.45 | 6.25 | 4.70 | 5.91 | 5.31 | 7.39 |
| $[0/\pm 55_2/90]_s$ | 4.78 | 5.14 | 4.96 | 6.27 | 5.07 | 6.13 | 5.60 | 9.72 |
| $[0/\pm 55/90_2]_s$ | 4.47 | 4.71 | 4.59 | 6.83 | 5.58 | 7.68 | 6.63 | 7.71 |

where $\overline{D}_0 = \overline{D}|_{s_n^\theta = s^{90} = s_0, \theta = 90}$, and the right-hand side of the equation represents the stiffness matrix of the damaged laminate expressed in terms of $E_1, E_2, G_{12}, \nu_{12}$ and $\nu_{21}$ evaluated at crack density $s_n^\theta = s^{90} = s_0$. Solving this equation the material constants of interest can be written as

$$a_1' = \frac{1}{2\overline{D}_0}\left[\frac{E_1}{1-\nu_{12}\nu_{21}} - \frac{E_1^0}{1-\nu_{12}^0\nu_{21}^0}\right]$$
$$a_2' = \frac{1}{2\overline{D}_0}\left[\frac{E_2}{1-\nu_{12}\nu_{21}} - \frac{E_2^0}{1-\nu_{12}^0\nu_{21}^0}\right] \quad (21)$$
$$a_4' = \frac{1}{\overline{D}_0}\left[\frac{\nu_{12}E_1}{1-\nu_{12}\nu_{21}} - \frac{\nu_{12}^0E_1^0}{1-\nu_{12}^0\nu_{21}^0}\right]$$

For the present study, we have calculated the constants $a_i'$ with FE data for the reference $[0/90_3]_s$ laminate with $s_0 = 1$ mm, given as: $E_1 = 0.675E_1^0, E_2 = E_2^0, \nu_{12} = 0.464\nu_{12}^0$. It is noted that the shear modulus for the cracked laminate can in principle be treated using Eq. (16) independent of the other moduli. But it needs evaluation of constant $a_3'$, which would require setting up a boundary value problem different from that needed to determine the other moduli. Hence, we shall not treat the shear modulus here.

#### 4.2.3. Predicted stiffness changes for $[0/\pm\theta/90]_s$ laminates

Finally, Eqs. (13)–(15) are used to predict the stiffness degradation in $[0/\pm\theta/90]_s$ laminates for different ply orientations. The comparison of SDM predictions and FE simulations for $\theta = 70, 55$ and $40^\circ$ are shown in Figs. 6–8. SDM predictions are made using CODs determined for interacting damage modes (i.e., both $\pm\theta$ and $90^\circ$ cracks present) as well as non-interacting damage modes. For $\theta = 70^\circ$ and $55^\circ$, SDM predictions agree reasonably well with FE simulations. However, for $\theta = 40^\circ$, SDM procedure predicts less severe degradation in axial modulus and in-plane Poisson's ratio than FE computations. This appears to be because the assumption in Eq. (A-23) is expected to limit the accuracy of the procedure to $\theta$-angles greater than $60^\circ$. However, the experimental studies (e.g., Varna et al., 1999; Tong et al., 1997a) have also shown that for axially loaded laminates, transverse cracks do not grow fully for ply orientations below $\theta = 55^\circ$ and the failure in laminates is actually induced by delamination.

It is important to note that in the present study, we have not considered the degradation of shear modulus due to shear deformation in off-axis plies. This is still a less-understood topic. However, one can include shear deformation

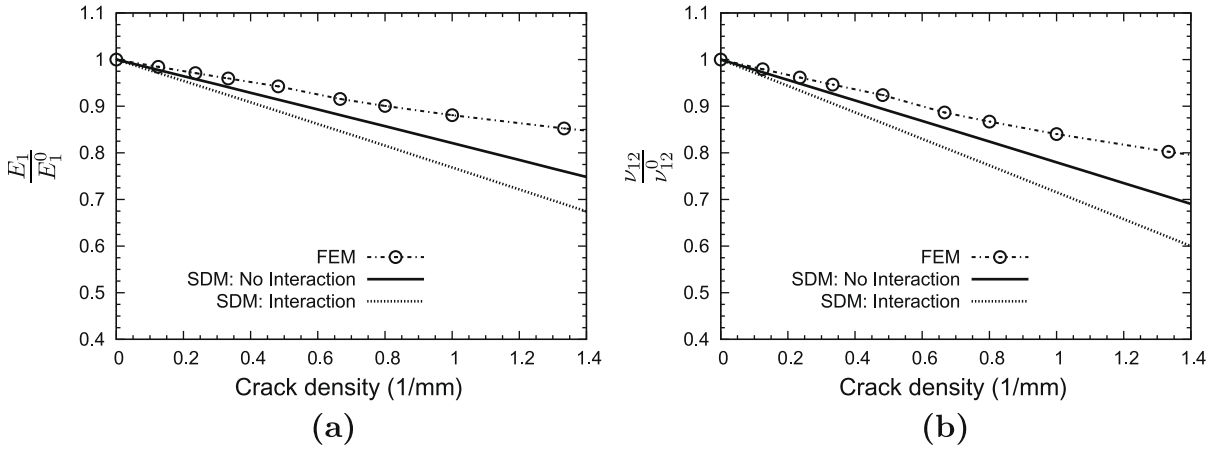


**Fig. 6.** Stiffness reduction for $[0/\pm 70/90]_s$ laminate compared with FE simulations. The crack density is along $X_1$ direction.

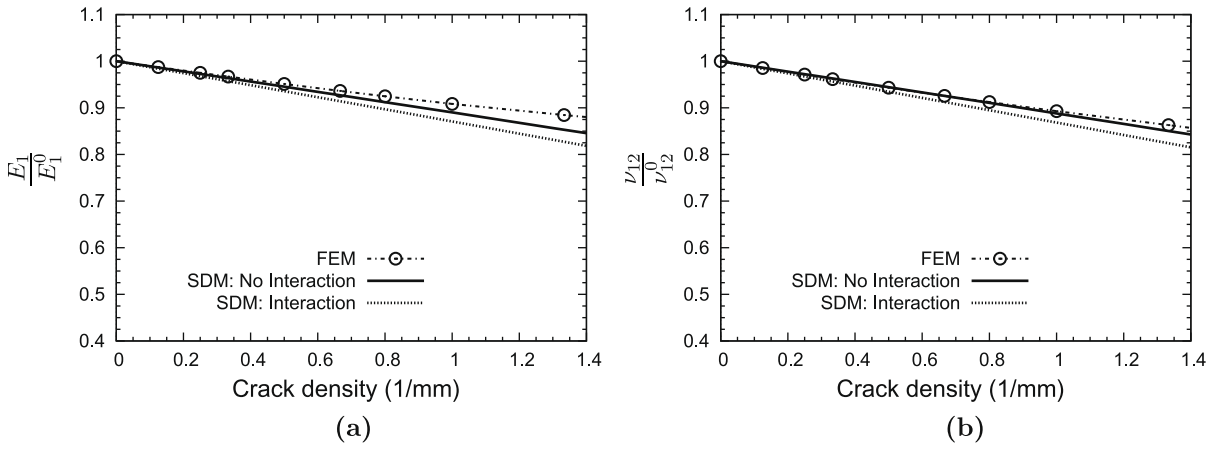


**Fig. 7.** Stiffness reduction for $[0/\pm 55/90]_s$ laminate compared with FE simulations.. The crack density is along $X_1$ direction.

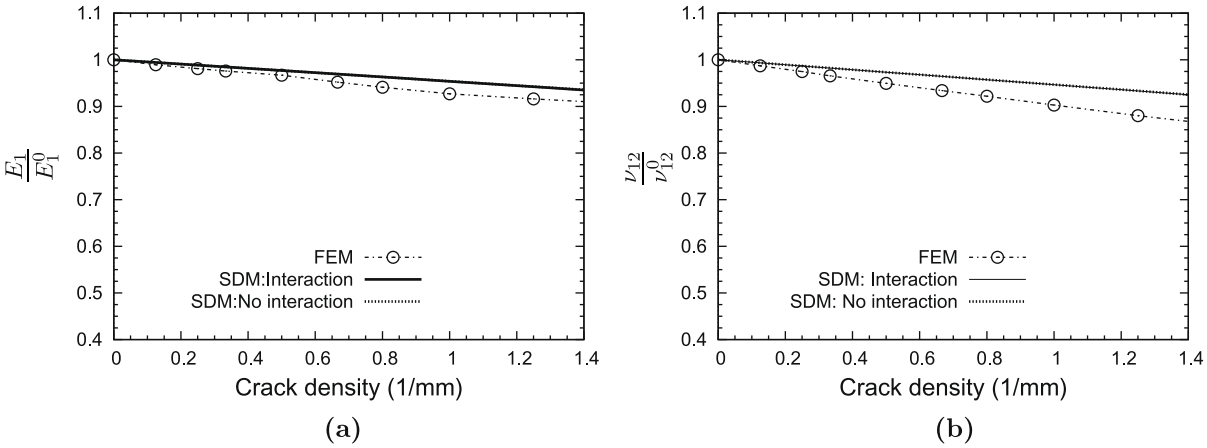


**Fig. 8.** Stiffness reduction for $[0/\pm 40/90]_s$ laminate compared with FE simulations. The crack density is along $X_1$ direction.

effects indirectly into SDM by using shear modulus variation with respect to applied loading as shown by Varna et al. Varna et al. (1999).

*4.2.4. Predictions for quasi-isotropic laminates*

The experimental data available for stiffness degradation in off-axis laminates involving cracks in multiple ply orientations under quasi-static loading are limited to quasi-isotropic laminates. Here we compare our predictions with the work by Tong et al. Tong et al. (1997a), who carried extensive measurements of stiffness degradation in $[0/90/\mp 45]_s$ glass-epoxy laminate. They observed partially initiated cracks in $\mp 45^\circ$-layers and plotted stiffness changes of the whole laminate as a function of 90°-cracking density.

For stiffness predictions using the SDM approach, the corresponding material constants $a_i'$ are evaluated from experimental data for $[0/90]_s$ laminate, shown in Fig. 9. The individual ply thickness for this laminate is 0.5 mm. This laminate corresponds to the $[0_m/90_r/\pm\theta_n]_s$ configuration for which the stiffness–damage relations are given in Eqs. (13)–(15), $\overline{D}$ is given in Eq. (10), and the constraint parameters are defined in Eq. (11). The normalized average CODs were again determined using FE analysis. The corresponding constraint parameters are calculated as: $\kappa_{90_{4n+2r}} = 6.1\text{e}{-3}, \kappa_\theta|_{\theta=90} \approx \kappa_{90} = 5.4\text{e}{-3}, \kappa_{\theta^+} = 3.97\text{e}{-3}, \kappa_{\theta^-} = 3.35\text{e}{-3}, \kappa_\theta = \frac{1}{2}(\kappa_{\theta^+} + \kappa_{\theta^-}) = 3.66\text{e}{-3}$.

In experiments Tong et al. (1997a) $\mp 45^\circ$-cracks did not grow fully and laminates failed by delamination. However, in FE analysis, we have assumed all cracks to be fully grown through laminate width. Now, the degradation effects due to cracks in a given layer (i.e., given crack size) should be directly proportional to the surface area of all the existing cracks. Thus, to account for partially grown cracks, we can reduce the crack density for that layer by a "relative density factor", defined as

$$\rho_r = \frac{\text{Actual surface area for partial cracks}}{\text{Surface area for full cracks}} \tag{22}$$

To find the actual surface area of partial cracks, the information regarding their actual length (along lamina width) is necessary. Since such data was not reported in

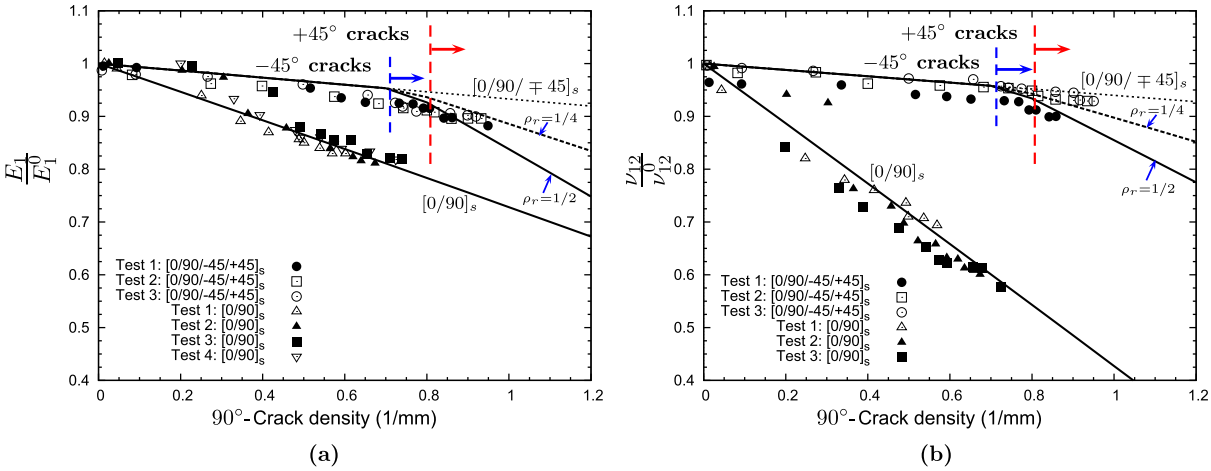


**Fig. 9.** Stiffness reduction for quasi-isotropic ($[0/90/\mp 45]_s$) laminate compared with experimental data Tong et al. (1997a). The damage constants are calculated using CDM for $[0/90]_s$ laminate. The crack density is along $X_1$ direction.

the above experimental study Tong et al. (1997a), we consider two cases. We assume that the $\mp 45$ cracks grow to half the laminate width in the first case and to $1/4^{th}$ in the latter, i.e., $\rho_r = 0.5, 0.25$, respectively.

SDM predictions for these cases using the FE computed CODs are shown against cracks density in 90°-ply in Fig. 9. The cracks in $-45°$-ply initiate at a cracks density of about 0.7 cracks/mm in 90°-ply, whereas the cracks in +45°-ply initiate about 0.8 cracks/mm. The dotted line for $[0/90/\mp 45]_s$ laminate represents damage in 90°-ply only. The SDM predictions for the two cases of partial cracks are shown for $\rho_r = 0.5$ and $\rho_r = 0.25$ by dashed and solid lines, respectively. The results for both axial modulus and Poisson's ratio are in very good agreement with the test data. The prediction with reduced crack density approaches a more realistic magnitude of stiffness degradation. The exact evaluation will, however, require the knowledge of crack length, their densities and evolution in each cracked layer with applied strain.

### 4.3. Parametric study

To seek further validation of the SDM procedure and to gain insight into the effects of relative thickness and stiffness of cracked vs. uncracked plies, we conduct a parametric study. The key again is numerical computation of constraint parameters. This can be attained by performing a suitable study of COD changes due to variation in material and geometry parameters of the laminate. Here, we carried out the study by varying the relative thickness of cracked and un-cracked layers for laminates in the class of $[0_m/\pm\theta_n/90_r]_s$ layup. The constants $a_i'$ are taken from previous analysis for the reference $[0/90_3]_s$ laminate. The comparison of SDM predictions for $m = 2, n = 2$ and $p = 2$ with numerical computations for a representative ply orientation, $\theta = 55°$, are shown respectively in Figs. 10–12. Except for the axial Poisson's ratio for $[0/\pm 55_2/90]_s$, the results show good agreement with FE simulations. Obviously, stiffness changes are most severe for $p = 2$ and least severe for $m = 2$. In fact, there is negligible difference in results for $m = 1$ and $m = 2$. Also, the interaction between damage modes increases as the thickness of cracked layer(s) increases. The general observation is that the thickness of cracked layer(s) has a significant impact on stiffness changes whereas increasing thickness of supporting plies has small effect on overall properties of the cracked laminate. The same observation was made for $[0_m/\pm\theta_n/0_{m/2}]_s$ laminates in Singh and Talreja (2008).

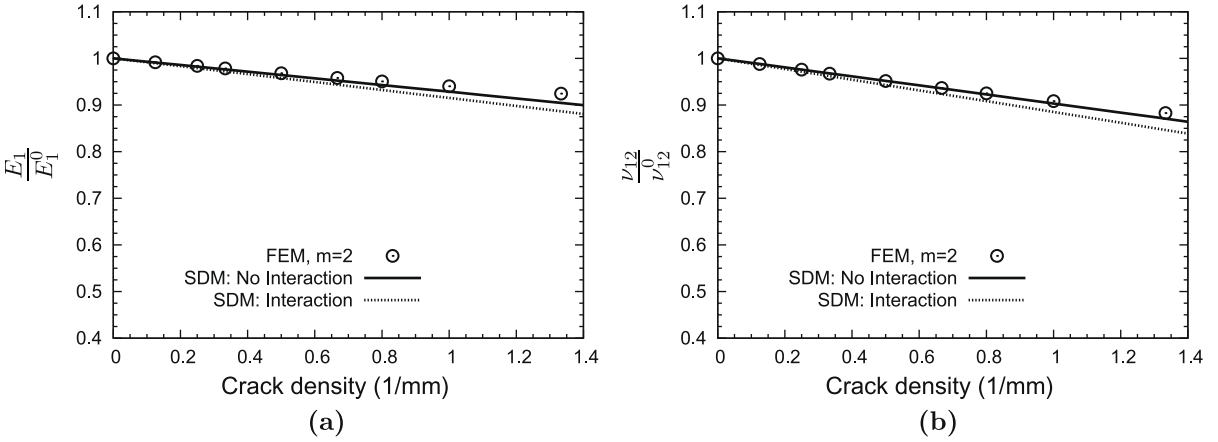


**Fig. 10.** Stiffness reduction for $[0_2/\pm 55/90]_s$ laminate compared with FE simulations. The crack density is along $X_1$ direction.

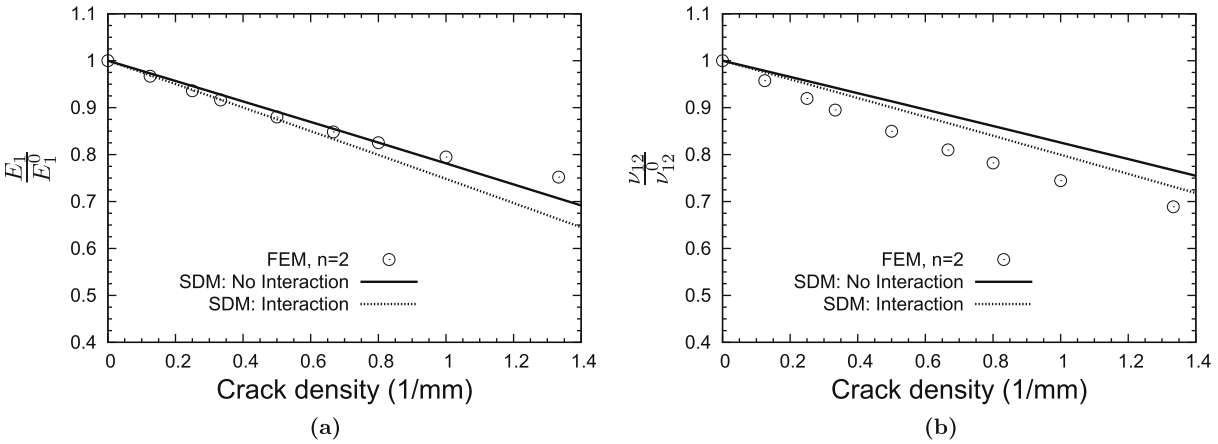


**Fig. 11.** Stiffness reduction for $[0/\pm 55_2/90]_s$ laminate compared with FE simulations. The crack density is along $X_1$ direction.

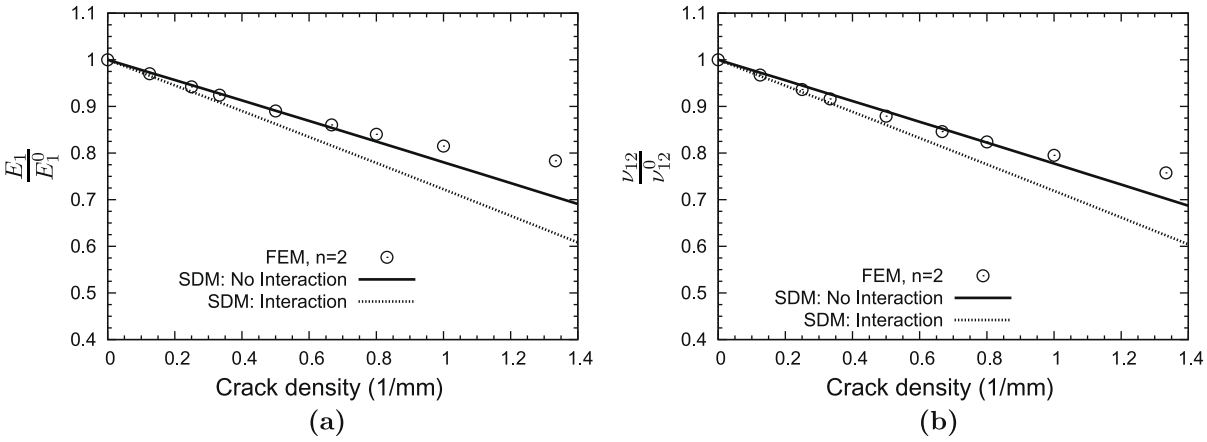


**Fig. 12.** Stiffness reduction for $[0/\pm 55/90_2]_s$ laminate compared with FE simulations. The crack density is along $X_1$ direction.

Similar parametric studies can also be used to evaluate stiffness changes with varying degree of relative material stiffnesses of un-cracked and cracked layers, e.g., if 0°-layer is made of different material than off-axis plies. These parametric studies enable efficient computations during design of laminated structures.

### 4.4. Discussion and assessment of the SDM approach for multi-mode damage

The stiffness–damage relationships (6), or equivalently, in engineering moduli form, Eqs. (13)–(16), provide the basis for predicting RVE-averaged stiffness properties for $[0_m/\pm\theta_n/90_r]_s$ laminates with simultaneous cracks in $+\theta$ and $-\theta$-plies, as well as in 90°-plies. These relationships, which are for an initially orthotropic laminate, state that the laminate is orthotropic also with ply cracks present. The procedures for calculating the damage parameter $\overline{D}$ and the damage-material constants $a_i'$ appearing in these equations have been described above. As noted above, we have treated the three coupled Eqs. (13)–(15), while Eq. (16), which involves shear response, has been left for future work. The shear response has been treated by other approaches, (e.g., Kashtalyan and Soutis, 2007).

While the predictions by the SDM approach can be viewed as satisfactory for changes in $E_1$ and $\nu_{12}$ for the class of laminates considered, as evidenced by comparisons in Figs. 6–12, it must be noted that the prediction of damage induced stiffness for multi-mode damage in general laminates is still a challenge. The previous work for $[0_m/\pm\theta_n/0_{m/2}]_s$ laminates (Singh and Talreja, 2008), and the current effort for $[0_m/\pm\theta_n/90_r]_s$ and $[0_m/90_r/\pm\theta_n]_s$ laminates, taken together, show a path forward to meeting that challenge. However, to proceed further, we must note the limitations in what has been accomplished in the present work. Firstly, the evaluation of the constraint parameters, as discussed in Section 4.2.1, requires calculating the average CODs from an FE model of the representative unit cell. The FE model shown in Fig. 3 is for an imposed uniform displacement in the axial direction. The CODs from this model allow evaluation of the constraint parameters that successfully lead to predictions of axial properties $E_1$ and $\nu_{12}$. Note that the assumption made in deriving Eq. (A-22), namely, $a_i \geqslant b_i$, is likely valid only for the case of axial loading of the laminate with damage. More work is needed to investigate the lateral loading case and to examine the associated prediction procedure for $E_2$ and $\nu_{21}$.

On the limitations side of the current SDM approach, we also note that the stiffness–damage relationships (Eq. (6)) are linear in the damage parameter as a consequence of restricting the polynomial expansion, Eq. (A-6), to linear terms in damage. This restriction can be easily relaxed at the cost of requiring more data for prediction of stiffness changes. It turns out, however, that the predictions by the linearized equations is quite satisfactory in most cases for crack densities of up to 1.0 cracks/mm, as seen in Figs. 6–12. In practical design one would seldom exceed such high crack densities, particularly when most cases examined experimentally show that delamination sets in when plies are cracked extensively. One more implication of the linearization is in evaluating the damage-material constants $a_i'$. As seen from Eq. (21), evaluation of these constants requires knowing changes in $E_1, E_2$ and $\nu_{12}$ for a selected cross ply laminate (here $[0/90_3]_s$), at one fixed crack density, as described in Section 4.2.2. Because of the linearization, while the actual stiffness dependence on damage is approximately linear, at least until reasonably high crack densities, the choice of the fixed crack density would affect the values of the $a_i'$ constants. It turns out however, that a prudent choice of 1.0 cracks/mm gives fairly accurate stiffness predictions, except perhaps for $\theta = 70^\circ$ as seen in Fig. 6.

The CDM formulation for constitutive relationships used here is based on a simplification stated early on in Talreja (1990) and having to do with crack surface displacements. Assuming brittle cracks whose formation and growth are governed by COD, the crack sliding displacement (CSD) was neglected. Thus, the quantity '$a$' in Eq. (1) represents COD. Later in a work related to damage in ceramic matrix composites Talreja (1991) the CSD was incorporated for fiber/matrix interfacial slip. Treating the COD and CSD separately significantly simplifies evaluation of the constraint parameter and leads to practical SDM methodologies for stiffness prediction. However, in using these methodologies caution should be exercised regarding where they are

applicable. In a work published after submission of our manuscript, Varna (2008) evaluated the effect of neglecting CSD in the SDM formulation. As expected, the prediction error is small for off-axis cracks at and near 90°, and increases with decreasing off-axis angle. It should be noted, however, that cracks are increasingly difficult to produce by an axial load as the off-angle angle decreases. It is further noted that the CSD cannot be neglected for shear-induced response, which has not been treated here.

## 5. Conclusions

The previously developed synergistic damage mechanics approach for $[0_m/\pm\theta_n/0_{m/2}]_s$ laminates in Singh and Talreja (2008) has been extended here for $[0_m/\pm\theta_n/90_r]_s$ and $[0_m/90_r/\pm\theta_n]_s$ laminates with cracks in 90°-plies in addition to the cracks in $+\theta$- and $-\theta$-plies. The extension is far from trivial, as the new case considered here has two distinct damage modes while in the previous case the two $\theta$ crack arrays could be treated equivalently as a single damage mode.

The stiffness–damage relationships for in-plane loading, derived for the current case of simultaneous presence of two damage modes subjected to enforced orthotropic symmetry of the cracked laminate, lead to four new damage related constants. A procedure for determining three of the constants, corresponding to axial loading, has been presented. Evaluation of these constants can be done from known stiffness changes of a cross ply laminate at a fixed crack density. These known stiffness values can be obtained experimentally, or, as demonstrated here, from a finite element model. A damage parameter representing the two simultaneous damage modes has been evaluated from a finite element model of the representative unit cell of the laminate containing damage by calculating the crack-surface averaged opening displacements. The stiffness predictions of independent cases using the evaluated material constants and the damage parameter show good agreement with directly calculated values by finite element models. Further validation of the prediction procedure comes from a parametric study of cracked and uncracked ply thicknesses.

Although the methodology developed here is still not fully general, the limitations being in linearization of the stiffness–damage relationships and in not considering shear loading, it is the first such treatment for multi-mode damage. Further work in the direction pursued is thought to provide further advance in treating damage of general laminates.

## Appendix

Here we derive the stiffness–damage relations for three modes of damage. With the damage mode tensors $D_{ij}^{(\alpha)}, \alpha = 1,2$ and 3, taken as internal variables, the Helmholtz free energy is given by

$$\rho\psi = \rho\psi\left(\epsilon_{ij}, D_{ij}^{(\alpha)}\right) \tag{A-1}$$

where $\psi$ is the specific Helmholtz energy, $\rho$ is the mass density, and $\epsilon_{ij}$ is the strain tensor. Using the second law of thermodynamics in the form of the Clausius-Duhem inequality, stress response for a given state of damage is given by Talreja (1990)

$$\sigma_{ij} = \rho\frac{\partial\psi}{\partial\epsilon_{ij}} \tag{A-2}$$

Utilizing the linear elastic stress–strain relation $\sigma_{ij} = C_{ijkl}\epsilon_{kl}$ for the composite material, its stiffness tensor $C_{ijkl}$ is given by

$$C_{ijkl} = \rho\frac{\partial^2\psi}{\partial\epsilon_{ij}\partial\epsilon_{kl}} \tag{A-3}$$

Composite laminates used in practice are usually symmetric and balanced about the mid-plane. Such stacking introduces an orthotropic symmetry of the laminate in its virgin state. To incorporate this material symmetry, the integrity bases (Adkins, 1960; Smith, 1982) are used to express $\rho\psi$ as a polynomial function. Here, we are interested in describing damage in $[0_m/\pm\theta_n/90_r]$ laminates with the following three damage modes

$$\begin{aligned}&\text{Damage Mode 1} \Rightarrow \alpha = 1, \text{cracks in } +\theta \text{ plies}\\ &\text{Damage Mode 2} \Rightarrow \alpha = 2, \text{cracks in } -\theta \text{ plies}\\ &\text{Damage Mode 3} \Rightarrow \alpha = 3, \text{cracks in } 90^\circ \text{ plies}\end{aligned}$$

For illustration purpose, we will first consider the laminate where the first two damage modes are active. Once we have formulated the stiffness matrix for this case, we will extend it to include the third damage mode as well. The irreducible integrity bases for a scalar polynomial function of symmetric second rank tensors (strain and two damage mode tensors) for this case ($\alpha = 1,2$) are given by Adkins (1960); Smith (1982)

$$\begin{aligned}&\epsilon_{11},\ \epsilon_{22},\ \epsilon_{33},\ \epsilon_{23}^2,\ \epsilon_{31}^2,\ \epsilon_{12}^2,\ \epsilon_{23}\epsilon_{31}\epsilon_{12},\\ &D_{11}^{(1)},\ D_{22}^{(1)},\ D_{33}^{(1)},\ \left(D_{23}^{(1)}\right)^2,\ \left(D_{31}^{(1)}\right)^2,\ \left(D_{12}^{(1)}\right)^2,\ D_{23}^{(1)}D_{31}^{(1)}D_{12}^{(1)},\\ &D_{11}^{(2)},\ D_{22}^{(2)},\ D_{33}^{(2)},\ \left(D_{23}^{(2)}\right)^2,\ \left(D_{31}^{(2)}\right)^2,\ \left(D_{12}^{(2)}\right)^2,\ D_{23}^{(2)}D_{31}^{(2)}D_{12}^{(2)},\\ &\epsilon_{23}D_{23}^{(1)},\ \epsilon_{31}D_{31}^{(1)},\ \epsilon_{12}D_{12}^{(1)},\ \epsilon_{23}D_{23}^{(2)},\ \epsilon_{31}D_{31}^{(2)},\ \epsilon_{12}D_{12}^{(2)},\\ &\epsilon_{31}\epsilon_{12}D_{23}^{(1)},\ \epsilon_{12}\epsilon_{23}D_{31}^{(1)},\ \epsilon_{23}\epsilon_{31}D_{12}^{(1)},\ \epsilon_{31}\epsilon_{12}D_{23}^{(2)},\ \epsilon_{12}\epsilon_{23}D_{31}^{(2)},\\ &\quad\epsilon_{23}\epsilon_{31}D_{12}^{(2)},\\ &\epsilon_{23}D_{31}^{(1)}D_{12}^{(1)},\ \epsilon_{31}D_{12}^{(1)}D_{23}^{(1)},\ \epsilon_{12}D_{23}^{(1)}D_{31}^{(1)},\ \epsilon_{23}D_{31}^{(2)}D_{12}^{(2)},\\ &\quad\epsilon_{31}D_{12}^{(2)}D_{23}^{(2)},\ \epsilon_{12}D_{23}^{(2)}D_{31}^{(2)},\\ &\epsilon_{23}D_{31}^{(1)}D_{12}^{(2)},\ \epsilon_{31}D_{12}^{(1)}D_{23}^{(2)},\ \epsilon_{12}D_{23}^{(1)}D_{31}^{(2)},\ \epsilon_{23}D_{31}^{(2)}D_{12}^{(1)},\\ &\quad\epsilon_{31}D_{12}^{(2)}D_{23}^{(1)},\ \epsilon_{12}D_{23}^{(2)}D_{31}^{(1)}\end{aligned} \tag{A-4}$$

If we consider a thin laminate loaded in its plane, this set of integrity bases can be further reduced by considering only the in-plane strain and damage tensor components. Thus, the remaining integrity bases in the Voigt notation, for the case with two damage modes, are given by

$$\begin{aligned}&\epsilon_1,\ \epsilon_2,\ \epsilon_6^2\\ &D_1^{(1)},\ D_2^{(1)},\ \left(D_6^{(1)}\right)^2,\ D_1^{(2)},\ D_2^{(2)},\ \left(D_6^{(2)}\right)^2\\ &\epsilon_6 D_6^{(1)},\ \epsilon_6 D_6^{(2)}\end{aligned} \tag{A-5}$$

where $\epsilon_1 \equiv \epsilon_{11}, \epsilon_2 \equiv \epsilon_{22}, \epsilon_6 \equiv \epsilon_{12}, D_1 \equiv D_{11}, D_2 \equiv D_{22}, D_6 \equiv D_{12}$. Using these integrity bases, the most general polynomial form for $\rho\psi$, restricted to second order terms in the strain components (small strains) and first-order terms in

damage tensor components (small volume fraction of damage entities in the RVE), is given by

$$\begin{aligned}\rho\psi = {} & P_0 + c_1\epsilon_1^2 + c_2\epsilon_2^2 + c_3\epsilon_6^2 + c_4\epsilon_1\epsilon_2 \\ & + \epsilon_1^2\left\{c_5 D_1^{(1)} + c_6 D_2^{(1)} + c_7 D_1^{(2)} + c_8 D_2^{(2)}\right\} \\ & + \epsilon_2^2\left\{c_9 D_1^{(1)} + c_{10} D_2^{(1)} + c_{11} D_1^{(2)} + c_{12} D_2^{(2)}\right\} \\ & + \epsilon_6^2\left\{c_{13} D_1^{(1)} + c_{14} D_2^{(1)} + c_{15} D_1^{(2)} + c_{16} D_2^{(2)}\right\} \\ & + \epsilon_1\epsilon_2\left\{c_{17} D_1^{(1)} + c_{18} D_2^{(1)} + c_{19} D_1^{(2)} + c_{20} D_2^{(2)}\right\} \\ & + \epsilon_1\epsilon_6\left\{c_{21} D_6^{(1)} + c_{22} D_6^{(2)}\right\} \\ & + \epsilon_2\epsilon_6\left\{c_{23} D_6^{(1)} + c_{24} D_6^{(2)}\right\} + P_1\left(\epsilon_p, D_q^{(1)}\right) \\ & + P_2\left(\epsilon_p, D_q^{(2)}\right) + P_3\left(D_q^{(1)}\right) + P_4\left(D_q^{(2)}\right) \end{aligned} \tag{A-6}$$

where $P_0$ and $c_i$ are material constants, $P_1$ and $P_2$ are linear functions of strain and damage tensor components, and $P_3$ and $P_4$ are linear functions only of the damage tensor components. Setting $\rho\psi = 0$ for unstrained and undamaged material, we have $P_0 = 0$; and assuming the unstrained material of any damaged state to be stress-free, we get $P_1 = P_2 = 0$ on using Eq. (A-2). Considering the virgin material to be orthotropic and proceeding in a similar manner as given in Talreja (1996), we obtain following relations for stiffness matrix of the damaged laminate

$$C_{pq} = C_{pq}^0 + C_{pq}^{(1)} + C_{pq}^{(2)} \tag{A-7}$$

where $p, q = 1, 2, 6$, $C_{pq}^0$ is the stiffness coefficient matrix of the virgin laminate and the changes in stiffness brought about by the individual damage modes are represented by $C_{pq}^{(1)}$ and $C_{pq}^{(2)}$. The three matrices are given by

$$C_{pq}^0 = \begin{bmatrix} 2c_1 & c_4 & 0 \\ c_4 & 2c_2 & 0 \\ 0 & 0 & 2c_3 \end{bmatrix} = \begin{bmatrix} \frac{E_1^0}{1-\nu_{12}^0\nu_{21}^0} & \frac{\nu_{12}^0 E_2^0}{1-\nu_{12}^0\nu_{21}^0} & 0 \\ \frac{\nu_{12}^0 E_2^0}{1-\nu_{12}^0\nu_{21}^0} & \frac{E_2^0}{1-\nu_{12}^0\nu_{21}^0} & 0 \\ 0 & 0 & G_{12}^0 \end{bmatrix} \tag{A-8}$$

$$C_{pq}^{(1)} = \begin{bmatrix} 2c_5 D_1^{(1)} + 2c_6 D_2^{(1)} & c_{17} D_1^{(1)} + c_{18} D_2^{(1)} & c_{21} D_6^{(1)} \\ & 2c_9 D_1^{(1)} + 2c_{10} D_2^{(1)} & c_{23} D_6^{(1)} \\ Symm & & 2c_{13} D_1^{(1)} + 2c_{14} D_2^{(1)} \end{bmatrix} \tag{A-9}$$

$$C_{pq}^{(2)} = \begin{bmatrix} 2c_7 D_1^{(2)} + 2c_8 D_2^{(2)} & c_{19} D_1^{(2)} + c_{20} D_2^{(2)} & c_{22} D_6^{(2)} \\ & 2c_{11} D_1^{(2)} + 2c_{12} D_2^{(2)} & c_{24} D_6^{(2)} \\ Symm & & 2c_{15} D_1^{(2)} + 2c_{16} D_2^{(2)} \end{bmatrix} \tag{A-10}$$

where $E_1^0, E_2^0, \nu_{12}^0$ and $\nu_{21}^0$ are longitudinal modulus, transverse modulus, and major and minor Poisson's ratios, respectively, for the virgin laminate.

Since we are dealing here with off-axis ply cracking, it is more convenient to rewrite the damage mode tensor defined in Eq. (4) in terms of normal crack spacing, $s_n^\theta = s_\theta \sin\theta$, where $s_\theta$ is the crack spacing in the axial direction (see Fig. 1) for the ply of orientation $\theta$. Accordingly, the damage tensor is given by

$$D_{ij}^{(\alpha)} = \frac{\kappa t_c^2}{s_n^\theta t} n_i n_j \tag{A-11}$$

With reference to Fig. 1(c) where the orientations of the two damage modes are shown and using Eq. (4), the damage tensor elements for this scenario are given by

$$\begin{aligned} & \alpha = 1 : n_i^{(1)} = (\sin\theta, \cos\theta, 0) \\ & D_1^{(1)} = \frac{\kappa^{\theta^+} t_c^2}{s_n^{\theta^+} t} \sin^2\theta;\ D_2^{(1)} = \frac{\kappa^{\theta^+} t_c^2}{s_n^{\theta^+} t} \cos^2\theta; \\ & D_6^{(1)} = \frac{\kappa^{\theta^+} t_c^2}{s_n^{\theta^+} t} \sin\theta\cos\theta \end{aligned} \tag{A-12}$$

$$\begin{aligned} & \alpha = 2 : n_i^{(2)} = (\sin\theta, -\cos\theta, 0) \\ & D_1^{(2)} = \frac{\kappa^{\theta^-} t_c^2}{s_n^{\theta^-} t} \sin\theta;\ D_2^{(2)} = \frac{\kappa^{\theta^-} t_c^2}{s_n^{\theta^-} t} \cos^2\theta; \\ & D_6^{(2)} = -\frac{\kappa^{\theta^-} t_c^2}{s_n^{\theta^-} t} \sin\theta\cos\theta \end{aligned} \tag{A-13}$$

where the superscripts $\theta^+$ and $\theta^-$ indicate variables for $+\theta$ and $-\theta$ plies, respectively. We now make an assumption that will be evaluated in the main text of the paper: the damage in $+\theta$-plies and $-\theta$-plies occurs at the same intensity of damage and it has the same effect on the laminate behavior. Thus,

$$\kappa^{\theta^+} = \kappa^{\theta^-} = \kappa_\theta, \quad s_n^{\theta^+} = s_n^{\theta^-} = s_n^\theta \tag{A-14}$$

With this assumption it follows that the laminate will retain its orthotropic symmetry, implying that the normal stress to shear stress coupling vanishes. Thus, from A-12, A-13, A-14 and using (A-7), (A-9) and (A-10), we get

$$\begin{aligned} & C_{11}^{(1)} + C_{11}^{(2)} = 2\frac{\kappa_\theta t_c^2}{s_n^\theta t}\left[(c_5 + c_7)\sin^2\theta + (c_6 + c_8)\cos^2\theta\right] \\ & C_{22}^{(1)} + C_{22}^{(2)} = 2\frac{\kappa_\theta t_c^2}{s_n^\theta t}\left[(c_9 + c_{11})\sin\theta + (c_{10} + c_{12})\cos^2\theta\right] \\ & C_{66}^{(1)} + C_{66}^{(2)} = 2\frac{\kappa_\theta t_c^2}{s_n^\theta t}\left[(c_{13} + c_{15})\sin^2\theta + (c_{14} + c_{16})\cos^2\theta\right] \\ & C_{12}^{(1)} + C_{12}^{(2)} = \frac{\kappa_\theta t_c^2}{s_n^\theta t}\left[(c_{17} + c_{19})\sin^2\theta + (c_{18} + c_{20})\cos^2\theta\right] \\ & C_{16}^{(1)} + C_{16}^{(2)} = \frac{\kappa_\theta t_c^2}{s_n^\theta t}\sin\theta\cos\theta[-c_{21} + c_{22}] = 0 \\ & C_{26}^{(1)} + C_{26}^{(2)} = \frac{\kappa_\theta t_c^2}{s_n^\theta t}\sin\theta\cos\theta[-c_{23} + c_{24}] = 0 \end{aligned} \tag{A-15}$$

Finally,

$$C_{pq}^{(1)} + C_{pq}^{(2)} = \begin{bmatrix} 2a_1 D_1 + 2b_1 D_2 & a_4 D_1 + b_4 D_2 & 0 \\ a_4 D_1 + b_4 D_2 & 2a_2 D_1 + 2b_2 D_2 & 0 \\ 0 & 0 & 2a_3 D_1 + 2b_3 D_2 \end{bmatrix} \tag{A-16}$$

where the superscripts for denoting damage mode have been dropped for convenience, and $a_i$ and $b_i, i = 1, 2, 3, 4$ are the two sets of four material constants, given by

$$\begin{aligned} & a_1 = c_5 + c_7; \quad a_2 = c_9 + c_{11}; \quad a_3 = c_{13} + c_{15}; \quad a_4 = c_{17} + c_{19} \\ & b_1 = c_6 + c_8; \quad b_2 = c_{10} + c_{12}; \quad b_3 = c_{14} + c_{16}; \quad b_4 = c_{18} + c_{20} \end{aligned} \tag{A-17}$$

Denote

$$\begin{aligned} a_1(\theta) &= a_1 \sin^2\theta + b_1 \cos^2\theta \\ a_2(\theta) &= a_2 \sin^2\theta + b_2 \cos^2\theta \\ a_3(\theta) &= a_3 \sin^2\theta + b_3 \cos^2\theta \\ a_4(\theta) &= a_4 \sin^2\theta + b_4 \cos^2\theta \end{aligned} \tag{A-18}$$

Then,

$$C^{(1)}_{pq} + C^{(2)}_{pq} = D_\theta \begin{bmatrix} 2a_1(\theta) & a_4(\theta) & 0 \\ & 2a_2(\theta) & 0 \\ Symm & & 2a_3(\theta) \end{bmatrix} \tag{A-19}$$

where

$$D_\theta = \frac{\kappa_\theta t_c^2}{s^\theta_n t} \tag{A-20}$$

Rewriting Eq. (A-18), as

$$a_i(\theta) = a_i \sin^2\theta + b_i \cos^2\theta = a_i \sin^2\theta \left(1 + \frac{b_i}{a_i}\cot^2\theta\right) \tag{A-21}$$

We now consider the case when $a_i \geq b_i$. Then,

$$\frac{b_i}{a_i}\cot^2\theta \leqslant 1 \quad \text{for} \quad \frac{\pi}{4} \leqslant \theta \leqslant \frac{\pi}{2} \tag{A-22}$$

Also, it can be expected that

$$\begin{aligned} &\frac{b_i}{a_i}\cot^2\theta \ll 1 \quad \text{for} \quad \frac{\pi}{3} \leqslant \theta \leqslant \frac{\pi}{2} \\ &i.e., \quad a_i(\theta) \approx a_i \quad \text{for} \quad \frac{\pi}{3} \leqslant \theta \leqslant \frac{\pi}{2} \end{aligned} \tag{A-23}$$

Considering now that additionally, we have cracks in the 90°-plies for which the damage mode $\alpha = 3$ has the following components

$$D^{(3)}_1 = \frac{\kappa_{90} t^2_{90}}{s^{90} t}, \; D^{(3)}_2 = D^{(3)}_6 = 0 \tag{A-24}$$

where $a'_i, i = 1,2,3,4$ are material constants. The integrity bases, Eq. (A-4), has an additional term $D^{(3)}_1$, and the free energy function gets the following additional terms,

$$\rho\psi(\alpha = 3) = a'_1\epsilon^2_1 D^{(3)}_1 + a'_2\epsilon^2_2 D^{(3)}_1 + a'_3\epsilon^2_6 D^{(3)}_1 + a'_4\epsilon_1\epsilon_2 D^{(3)}_1 \tag{A-25}$$

Following the steps taken above, we get

$$\begin{aligned} &C^{(3)}_{11} = 2a'_1 D^{(3)}_1, \quad C^{(3)}_{22} = 2a'_2 D^{(3)}_1 \\ &C^{(3)}_{12} = a'_4 D^{(3)}_1, \quad C^{(3)}_{66} = 2a'_3 D^{(3)}_1 \\ &C^{(3)}_{16} = C^{(3)}_{26} = 0 \end{aligned} \tag{A-26}$$

It is noted here that for $[0_m/\pm\theta_n/90_r]_s$ laminate, $\pm\theta$-modes occur twice (below and above the laminate midplane) whereas the central 90°-mode occurs only once. Thus, the total stiffness change $\Delta C_{pq}$ with all the three modes active is given by

$$\begin{aligned} \Delta C_{pq} =& 2\left\{C^{(1)}_{pq} + C^{(2)}_{pq}\right\} + C^{(3)}_{pq} = 2D_\theta \begin{bmatrix} 2a_1 & a_4 & 0 \\ a_4 & 2a_2 & 0 \\ 0 & 0 & 2a_3 \end{bmatrix} \\ &+ D_{90} \begin{bmatrix} 2a'_1 & a'_4 & 0 \\ a'_4 & 2a'_2 & 0 \\ 0 & 0 & 2a'_3 \end{bmatrix} \end{aligned} \tag{A-27}$$

where

$$D_{90} = D^{(3)}_1 = \frac{\kappa_{90} t^2_{90}}{s^{90} t} \tag{A-28}$$

and Eq. (A-23) has been used.

Now consider $\theta = 90^\circ$ in the $[0_m/\pm\theta_n/90_r]_s$ laminate. Let the normal crack spacing be the same in all cracked plies, i.e., $s^{\theta^+}_n = s^{\theta^-}_n = s^{90}$. Then, the terms of $\Delta C_{pq}$ matrix become, as illustrated by $\Delta C_{11}$ as

$$\begin{aligned} \Delta C_{11} &= 2\left\{C^{(1)}_{11} + C^{(2)}_{11}\right\} + C^{(3)}_{11} = 4D_\theta|_{\theta=90} a_1(90) + 2D_{90}a'_1 \\ &= \frac{4\kappa_{\theta=90}(t_0.2n)^2}{s^{90}t} a_1(90) + \frac{2\kappa_{90}(t_0.2r)^2}{s^{90}t} a'_1 \qquad \text{(A- 29)} \\ &= \frac{8t_0^2}{s^{90}t}\left[2n^2\kappa_{\theta=90}a_1(90) + r^2\kappa_{90}a'_1\right] \qquad \text{(A-30)} \end{aligned}$$

where $t_0$ is a single ply thickness. We can consider this stiffness change to be the same as that for a $[0_m/90_{2n+r}]_s$ laminate with a single mode of damage given by

$$D_1 = \frac{\kappa_{90_{4n+2r}} t_0^2.\{(4n+2r)\}^2}{s^{90}t} \tag{A-31}$$

where the sub-subscript on $\kappa_{90}$ denotes the crack size. The stiffness change $\Delta C_{11}$ will then be

$$\Delta C_{11} = 2a'_1 D_1 = \frac{8t_0^2}{s^{90}t}(2n+r)^2\kappa_{90_{4n+2r}}a'_1 \tag{A-32}$$

Equating $\Delta C_{11}$ from Eqs. (A-30) and (A-32), we have

$$2n^2\kappa_\theta|_{\theta=90}a_1(90) + r^2\kappa_{90}a'_1 = (2n+r)^2\kappa_{90_{4n+2r}}a'_1 \tag{A-33}$$

Solving the above equation, we obtain

$$a_1(90) = \left[\frac{(2n+r)^2\kappa_{90_{4n+2r}} - r^2\kappa_{90}}{2n^2\kappa_\theta|_{\theta=90}}\right]a'_1 \tag{A-34}$$

Thus, the inter-relation between $a_i$ and $a'_i$ constants is given by

$$a_i = \left[\frac{(2n+r)^2\kappa_{90_{4n+2r}} - r^2\kappa_{90}}{2n^2\kappa_\theta|_{\theta=90}}\right]a'_i \tag{A-35}$$

Substituting (A-35) into (A-27), we obtain $\Delta C_{pq}$ for damaged $[0_m/\pm\theta_n/90_r]_s$ laminate as

$$\begin{aligned} \Delta C_{pq} &= 2\left\{C^{(1)}_{pq} + C^{(2)}_{pq}\right\} + C^{(3)}_{pq} = \frac{4t_0^2}{t}\left[2n^2\frac{\kappa_\theta}{s^\theta_n}[a_i] + r^2\frac{\kappa_{90}}{s^{90}}[a'_i]\right] \\ &= \frac{4t_0^2}{t}\left[\frac{1}{s^\theta_n}\frac{\kappa_\theta}{\kappa_\theta|_{\theta=90}}\{(2n+r)^2\kappa_{90_{4n+2r}} - r^2\kappa_{90}\} + r^2\frac{\kappa_{90}}{s^{90}}\right][a'_i] \end{aligned} \tag{A-36}$$

where $[a_i]$ and $[a'_i]$ represent the coefficient matrices, appearing as multiplying factors to $2D_\theta$ and $D_{90}$, respectively, in Eq. (A-27).

Thus, the entire stiffness matrix is given by

$$C_{pq} = \begin{bmatrix} \frac{E_1^0}{1-\nu_{12}^0\nu_{21}^0} & \frac{\nu_{12}^0 E_2^0}{1-\nu_{12}^0\nu_{21}^0} & 0 \\ & \frac{E_2^0}{1-\nu_{12}^0\nu_{21}^0} & 0 \\ Symm & & G_{12}^0 \end{bmatrix} + \overline{D}\begin{bmatrix} 2a_1' & a_4' & 0 \\ & 2a_2' & 0 \\ Symm & & 2a_3' \end{bmatrix} \tag{A-37}$$

where

$$\overline{D} = \frac{4t_0^2}{t}\left[\frac{1}{s_n^\theta}\frac{\kappa_\theta}{\kappa_\theta|_{\theta=90}}\{(2n+r)^2\kappa_{90_{4n+2r}} - r^2\kappa_{90}\} + r^2\frac{\kappa_{90}}{s^{90}}\right] \tag{A-38}$$

## References


Adkins, J., 1960. Symmetry relations for orthotropic and transversely isotropic materials. Arch. Rational Mech. Anal. 4, 193–213.

Gudmundson, P., Ostlund, S., 1992. First order analysis of stiffness reduction due to matrix cracking. J. Compos. Mater. 26 (7), 1009–1030.

Gudmundson, P., Zang, W.L., 1993. An analytic model for thermoelastic properties of composite laminates containing transverse matrix cracks. Int. J. Solids Struct. 30 (23), 3211–3231.

Kashtalyan, M., Soutis, C., 2000a. The effect of delaminations induced by transverse cracks and splits on stiffness properties of composite laminates 31 (2), 107–119.

Kashtalyan, M., Soutis, C., 2000b. Modelling stiffness degradation due to matrix cracking in angleply composite laminates. Plast. Rubber Compos. 29 (9), 482–488.

Kashtalyan, M., Soutis, C., 2000c. Stiffness degradation in cross-ply laminates damaged by transverse cracking and splitting 31 (4), 335–351.

Kashtalyan, M., Soutis, C., 2007. Stiffness and fracture analysis of laminated composites with off-axis ply matrix cracking. Composites A: Appl. Sci. Mfg. 38 (4), 1262–1269.

Lundmark, P., Varna, J., 2005. Constitutive relationships for laminates with ply cracks in in-plane loading. Int. J. Dam. Mech. 14 (3), 235–259.

Lundmark, P., Varna, J., 2006. Crack face sliding effect on stiffness of laminates with ply cracks. Compos. Sci. Tech. 66 (10), 1444–1454.

Masters, J., Reifsnider, K., 1982. An investigation of cumulative damage development in quasi-isotropic graphite/epoxy laminates. In: Reifsnider, K. (Ed.), Damage in Composite Materials. ASTM STP, pp. 40–62.

National Research Council, Committee on Durability and Life Prediction of Polymer Matrix Composites in Extreme Environments, 2005. Going to Extremes: Meeting the Emerging Demand for Durable Polymer Matrix Composites. National Academies Press.

O'Brien, T., Hooper, S. (Eds.), 1993. Composite Materials: Fatigue and Fracture. ASTM STP, Philadelphia.

Singh, C.V., Talreja, R., 2008. Analysis of multiple off-axis ply cracks in composite laminates. Int. J. Solids Struct. 45 (16), 4574–4589.

Smith, G.F., 1982. On transversely isotropic functions of vectors, symmetric 2nd-order tensors and skew-symmetric 2nd-order tensors. Q Appl. Math. 39 (4), 509–516.

Talreja, R., 1990. Internal variable damage mechanics of composite materials. In: Boehler, J.P. (Ed.), Yielding, Damage, and Failure of Anisotropic Solids. Mechanical Engineering Publications, London, pp. 509–533.

Talreja, R., 1991. Continuum modeling of damage in ceramic matrix composites. Mech. Mater. 12 (2), 165–180.

Talreja, R., 1994. Damage characterization by internal variables. In: Talreja, R. (Ed.), Damage Mechanics of Composite Materials. Elsevier, Amsterdam, pp. 53–78.

Talreja, R., 1996. A synergistic damage mechanics approach to durability of composite material systems. In: Cardon, A., Fukuda, H., Reifsnider, K. (Eds.), Progress in Durability Analysis of Composite Systems. A.A. Balkema, Rotterdam, pp. 117–129.

Tong, J., Guild, F.J., Ogin, S.L., Smith, P.A., 1997a. On matrix crack growth in quasi-isotropic laminates – I. Experimental investigation. Compos. Sci. Tech. 57 (11), 1527–1535.

Tong, J., Guild, F.J., Ogin, S.L., Smith, P.A., 1997b. On matrix crack growth in quasi-isotropic laminates – II. Finite element analysis. Compos. Sci. Tech. 57 (11), 1537–1545.

Varna, J., 2008. Physical interpretation of parameters in synergistic continuum damage mechanics model for laminates. Compos. Sci. Tech. 68 (13), 2592–2600.

Varna, J., Joffe, R., Akshantala, N.V., Talreja, R., 1999. Damage in composite laminates with off-axis plies. Compos. Sci. Tech. 59 (14), 2139–2147.

Yokozeki, T., Aoki, T., 2005. Overall thermoelastic properties of symmetric laminates containing obliquely crossed matrix cracks. Compos. Sci. Tech. 65 (11-12), 1647–1654.

Zhang, J., Herrmann, K., 1999. Stiffness degradation induced by multilayer intralaminar cracking in composite laminates. Composites A: Appl. Sci. Mfg. 30 (5), 683–706.

Zhang, J., Fan, J., Soutis, C., 1992. Analysis of multiple matrix cracking in [+/-theta(m)/90(n)]s composite laminates. 1. In-plane stiffness properties. Composites 23 (5), 291–298.